

Title	Phase-amplitude coupling of ripple activities during seizure evolution with theta phase
Author(s)	Hashimoto, Hiroaki; Khoo, Hui Ming; Yanagisawa, Takufumi et al.
Citation	Clinical Neurophysiology. 2021, 132(6), p. 1243-1253
Version Type	AM
URL	https://hdl.handle.net/11094/95539
rights	©2021. This manuscript version is made available under the CC-BY-NC-ND 4.0 license
Note	

Osaka University Knowledge Archive : OUKA

<https://ir.library.osaka-u.ac.jp/>

Osaka University

1 **Phase-amplitude coupling of ripple activities during seizure evolution with**
2 **theta phase**

3

4 Hiroaki Hashimoto. M.D., Ph.D.^{1,2,3*}, Hui Ming Khoo. M.D., Ph.D.⁴, Takufumi Yanagisawa.

5 M.D., Ph.D.⁴, Naoki Tani. M.D., Ph.D.⁴, Satoru Oshino. M.D., Ph.D.⁴, Haruhiko Kishima.

6 M.D., Ph.D.⁴, Masayuki Hirata. M.D., Ph.D.^{1,3,4}

7

8 ¹ Department of Neurological Diagnosis and Restoration, Graduate School of Medicine,
9 Osaka University, Suita 565-0871, Japan

10 ² Department of Neurosurgery, Otemae Hospital, Osaka, 540-0008, Japan

11 ³ Endowed Research Department of Clinical Neuroengineering, Global Center for Medical
12 Engineering and Informatics, Osaka University, Suita 565-0871, Japan

13 ⁴ Department of Neurosurgery, Graduate School of Medicine, Osaka University, Suita 565-
14 0871, Japan

15

16 *** Correspondence:**

17 Hiroaki Hashimoto, M.D., Ph.D.

18 Invited Researcher, Department of Neurological Diagnosis and Restoration, Graduate School
19 of Medicine, Osaka University, Yamadaoka 2-2, Suita, Osaka, Japan

20 Tel.: +81-6-6210-8429

21 Fax: +81-6-6210-8430

22 E-mail: h-hashimoto@ndr.med.osaka-u.ac.jp

23

24

25 **Key Words:** Seizures; Phase-amplitude coupling; Theta band; Visualization; High-frequency
26 activities; Intracranial EEG;

27

28 **Highlights**

29 • We visualized the phase-amplitude coupling phenomenon related to seizures by showing
30 rhythmic fluctuation of high-frequency activities.

31 • The low frequency band mainly coupled ictal-ripple activities was the θ band (4–8 Hz).

- 32 • The seizure-related ripple power started to increase, and then spread, with fluctuations,
33 and not with linear increases.

34

35 **Abstract**

36 **Objective**

37 High-frequency activities (HFAs) and phase-amplitude coupling (PAC) are key
38 neurophysiological biomarkers for studying human epilepsy. We aimed to clarify and visualize
39 how HFAs are modulated by the phase of low-frequency bands during seizures.

40 **Methods**

41 We used intracranial electrodes to record seizures of focal epilepsy (12 focal-to-bilateral tonic-
42 clonic seizures and three focal-aware seizures in seven patients). The synchronization index,
43 representing PAC, was used to analyze the coupling between the amplitude of ripples (80–250
44 Hz) and the phase of lower frequencies. We created a video in which the intracranial electrode
45 contacts were scaled linearly to the power changes of ripple.

46 **Results**

47 The main low frequency band modulating ictal-ripple activities was the θ band (4–8 Hz), and
48 after completion of ictal-ripple burst, δ (1–4 Hz)-ripple PAC occurred. The ripple power
49 increased simultaneously with rhythmic fluctuations from the seizure onset zone, and spread
50 to other regions.

51 **Conclusions**

52 Ripple activities during seizure evolution were modulated by the θ phase. The PAC
53 phenomenon was visualized as rhythmic fluctuations.

54 **Significance**

55 Ripple power associated with seizure evolution increased and spread with fluctuations. The θ
56 oscillations related to the fluctuations might represent the common neurophysiological
57 processing involved in seizure generation.

58

59 *Abbreviations:*

60 CT, Computerized tomography; EEG, Electroencephalograms; FAS, Focal aware seizure;
61 FBTCS, Focal to bilateral tonic-clonic seizures; FIAS, Focal impaired awareness seizure;
62 FLAIR, Fluid-attenuated inversion recovery; FWE, Familywise error; HFAs, High-frequency
63 activities; HFOs, High frequency oscillations; iEEG, Intracranial electroencephalograms; MRI,
64 Magnetic resonance imaging; MTL, Mesial temporal lobe; P, Patient; PAC, Phase-amplitude
65 coupling; PRC, Preceding ripple contact; S, Seizure; SD, Standard deviation; SI,
66 Synchronization index; SIm, Synchronization index magnitude; SImb, Bootstrapping
67 synchronization index magnitude; SO, Seizure onset; SOC, Seizure onset contact; SOZ,
68 Seizure onset zone; 3D, Three-dimensional;

69

Preprint

70 **1. Introduction**

71 Intracranial electroencephalograms (iEEG) allow acquisition of wideband waveforms,
72 from slow shift to high-frequency activities (HFAs), at a high signal-to-noise ratio. Direct
73 current (DC) shifts and infraslow activities, which are very slow-frequency components,
74 appear in the seizure onset zone (SOZ) during a seizure (Ikeda et al., 1999, Imamura et al.,
75 2011, Kanazawa et al., 2015, Rodin and Modur, 2008). HFAs can be physiological, i.e., those
76 recorded during a task (Hashimoto et al., 2017, Hashimoto et al., Hashimoto et al., 2020b), or
77 pathological, i.e., those observed during seizures or interictal period in epileptic patients
78 (Akiyama et al., 2006, Imamura et al., 2011, Zijlmans et al., 2012). High frequency oscillations
79 (HFOs) are subgroup of HFAs and isolated oscillations standing out from the background,
80 within the high frequency range usually above 80 Hz. Ictal HFOs occur in the SOZ (Jirsch et
81 al., 2006, Modur et al., 2011), and HFOs can be further classified into ripples (80–250 Hz) and
82 fast ripples (250–500 Hz) (Modur et al., 2011). Previous study reported that HFAs were useful
83 for detection of seizures (Ayoubian et al., 2013).

84

85 The amplitude of HFAs is modulated by the low-frequency oscillation phase (Canolty
86 et al., 2006). Physiologically, this phase-amplitude coupling (PAC) has various functional roles
87 in cortical processing such as motor execution (Yanagisawa et al., 2012) and sensory
88 processing (Luo and Poeppel, 2007). In the ictal state, PAC achieved high values in the SOZ
89 (Ibrahim et al., 2014, Iimura et al., 2018). Moreover, it is reported that PAC between the
90 infraslow phase and HFAs amplitude preceded the seizure onset (SO) (Hashimoto et al., 2020a).

91

92 PAC achieves high values in the SOZ during seizures; however, there is no consensus
93 about the main low frequency band that modulates the amplitude of HFAs. Several low
94 frequency bands have been reported like δ (Iimura et al., 2018, Nariai et al., 2011, Nonoda et
95 al., 2016), θ (Ibrahim et al., 2014), α (Ibrahim et al., 2014), and β (Edakawa et al., 2016) bands.

96 Furthermore, whereas dynamic HFAs changes in the ictal state have been visualized using
97 topographic videos (Akiyama et al., 2006), dynamic PAC changes have not been visualized.
98 The purpose of this study is twofold. One is to clearly identify the main low frequency band
99 contributing to PAC during seizures. The other is to visualize the PAC phenomenon. Using the
100 iEEG, we collected data from 15 seizures in seven patients with medically refractory focal
101 epilepsy. Twelve focal-to-bilateral tonic-clonic seizures (FBTCS), and three focal-aware
102 seizures (FAS) were investigated. First, we evaluated dynamic changes and characteristics of
103 PAC from pre-ictal to late-ictal. Next, we created a video for each patient in which circles,
104 corresponding to electrodes, change their diameters that correlate linearly with the power of
105 HFAs represented by ripples (Video 1–3). We hypothesized that PAC can be visualized using
106 dynamic ripple power changes modulated by a low-frequency band.

107

108

109 **2. Materials and Methods**

110

111 *2.1. Subjects*

112 We enrolled patients with drug-resistant focal epilepsy who underwent intracranial
113 electrodes placement for presurgical invasive electroencephalograms (EEG) study who were
114 admitted to Osaka University Hospital from July 2018 to July 2019. This retrospective study
115 was approved by the Ethics Committee of Osaka University Hospital (Suita, Japan) (approval
116 no., 19193). Informed consent was obtained by the opt-out method on our center's website.

117

118 *2.2. Intracranial electrodes and their location*

119 Data on iEEG were acquired using a combination of subdural grids (10, 20, or 30
120 contacts), strips (four or six contacts), and depth electrodes (six contacts) (Unique Medical Co.
121 Ltd., Tokyo, Japan), placed using conventional craniotomy. The diameter of each contact was

122 3 or 5 mm, and the inter-contact distance was 5, 7, or 10 mm for grid and strip electrodes. The
123 diameter was 1.5 mm, and the inter-contact distance was 5 mm for depth electrodes. Three-
124 dimensional (3D) brain renderings were created using FreeSurfer
125 (<https://surfer.nmr.mgh.harvard.edu>) with the preoperative magnetic resonance imaging (MRI)
126 images. Using Brainstorm (<http://neuroimage.usc.edu/brainstorm/>), the post-implantation
127 computerized tomography (CT) images were overlaid onto the 3D brain renderings to obtain
128 the position of contact for each electrode in the Montreal Neurological Institute coordinates
129 system.

130

131 *2.3. Data acquisition and preprocessing*

132 Signals from the iEEG were acquired at a sampling rate of 1 kHz and a time constant
133 of 10 s, using a 128-channel digital EEG system (EEG 2000; Nihon Kohden Corporation,
134 Tokyo, Japan). The raw signals were then preprocessed using a low-pass filter at 333 Hz (to
135 prevent aliasing) and a 60-Hz notch filter (to eliminate the alternating current line artifact)
136 using the BESA Research 6.0 software (BESA GmbH, Grafelfing, Germany). Artifactual
137 signals from electrodes were excluded from further analyses. For the purpose of signal analysis,
138 iEEG signal of each electrode contact was digitally re-referenced to a common average of all
139 electrode contacts in each patient.

140 All the subsequent signal analysis was performed using MATLAB R2019b
141 (MathWorks, Natick, MA, USA). Our iEEG data were saved every 60 min and thus each iEEG
142 dataset contains a 60-min signal. A bandpass filter using a two-way least-squares finite impulse
143 response filter (`pop_eegfiltnew.m` from the EEGLAB toolbox,
144 <https://sccn.ucsd.edu/eeglab/index.php>) was applied to the preprocessed signals of the whole
145 60-min data to prevent edge-effect artifacts, before we extract iEEG segments for subsequent
146 signal analysis.

147

148 *2.4. Seizure onset contact (SOC)*

149 The SO were determined by visual inspections of iEEG signals using low-voltage fast
150 activity (Perucca et al., 2014), disappearance of the background activity (Ikeda et al., 1999),
151 and DC shifts (Ikeda et al., 1996) et al. We defined the SOC as contacts that showed initial
152 epileptic iEEG changes. If one patient with more than one seizure exhibited several SOC which
153 fulfilled the condition, and the contacts were commonly involved at seizure onset across all
154 seizures, then we randomly selected one contact in order to simplify the analysis (Fig. 1A).

155

156 *2.5. High frequency activity power changes*

157 We analyzed the iEEG data acquired 5 minutes before and after the SO for each
158 recorded seizure. We used the ripple band (80–250 Hz) to represent HFA. The time series of
159 the HFA power on each contact was constructed every second from the preprocessed iEEG
160 signal by using a band-pass filter (80–250 Hz) in combination with the Hilbert transformation
161 (Cohen, 2008). The HFA power was then normalized by dividing the power at each second by
162 the average HFA power of the initial 60 s.

163

164 *2.6. Preceding ripple contact (PRC)*

165 *Preceding* ripple activities were observed as a cluster after the SO if the ripple
166 normalized power exceeded 10, continued for more than a few seconds, and preceded the later
167 ripple activities. We defined contacts that showed the preceding ripple activities as PRC (Fig.
168 1B). Moreover, we investigated whether the SOC matched the PRC (SOC-PRC concordance;
169 Table 1).

170

171 *2.7. PAC analyses*

172 We used synchronization index (SI) (Cohen, 2008) to measure the strength of cross-
173 frequency coupling between the amplitude of ripple and the phases of lower frequency bands,

174 which include δ (1–4 Hz), θ (4–8 Hz), α (8–13 Hz), and β (13–30 Hz).

175 Hilbert transformation was performed on the bandpass filtered signals to obtain the complex-
176 valued analytic signals of each frequency band, $Z_\omega(t)$ (ω means the frequency band). For each
177 frequency band, the amplitude, $A_\omega(t)$, and phase, $\phi_\omega(t)$, were calculated from the complex-
178 valued signals using Equation 1.

$$179 \quad Z_\omega(t) = A_\omega(t) \cdot \exp(i \phi_\omega(t)) \quad (1)$$

180 The phase of each lower frequency band, $\phi_l(t)$, was obtained from the angle of the Hilbert
181 transform of the bandpass filtered signal.

182 To obtain the surrogate signal that represent the time series of the ripple band
183 amplitude, the amplitude of ripple band was first extracted using the squared magnitude of
184 $Z_\gamma(t)$, the analytic signal calculated using the Hilbert transformation ($P_\gamma(t) = \text{real}[Z_\gamma(t)]^2 +$
185 $\text{image}[Z_\gamma(t)]^2$); then the phase of this amplitude was computed using Hilbert transformation
186 ($\phi_\gamma(t) = \arctan(\text{image}[Z(P_\gamma(t))]/\text{real}[Z(P_\gamma(t))])$).

187 SI was calculated using Equation 2.

$$188 \quad SI = \frac{1}{n} \times \sum_{t=1}^n e^{i[\phi_l(t) - \phi_\gamma(t)]} \quad (2)$$

189 We calculated SI for every 1-s time window, which sequentially shifted every 33 ms
190 from 5 minutes before to 5 minutes after the SO. n is the number of time points within each 1-
191 s time window. SI is a complex number; therefore, we used the magnitude of SI, referred to as
192 SIm. SIm varies between 0 and 1, with 0 indicating that phases are completely desynchronized
193 and 1 indicating that phases are perfectly synchronized.

194

195 2.8. Correlation analysis related to PAC

196 We analyzed the correlation between SIm and ripple normalized power in the
197 following three states in relation to seizure onset: pre-ictal (from -1.5 to 0 min before the SO),
198 ictal (from 0 to 1.5 min after the SO), and late-ictal (from 1.5 to 3.0 min after the SO) states

199 using implanted all contacts (total 1189 electrode contacts). Pearson correlation coefficients
200 were calculated.

201

202 *2.9. Phase-conditioned analysis*

203 To identify the lower frequency phase to which ripple power was coupled, we
204 computed the average oscillation of each lower frequency band on the SOC across all seizures
205 (15 seizures) and the average ripple normalized power on the SOC. The phases of δ and θ band,
206 were divided into 12 intervals of 30° without overlaps: $0^\circ \pm 15^\circ$, $30^\circ \pm 15^\circ$, ..., $300^\circ \pm 15^\circ$, and
207 $330^\circ \pm 15^\circ$, resulting in 12 phase bins. The reason for choosing these two bands is described in
208 the result section. For each state (pre-ictal, ictal, and late-ictal), the ripple normalized power
209 on the SOC was averaged within each phase bin. Using signal from the SOC instead of the
210 average of all electrode contacts avoids averaging from obscuring the characteristics-of-interest.

211

212 *2.10. Visualization of synchronized multimodal data*

213 Multimodal data, including iEEG waveform, ripple normalized power, and SIm, were
214 synchronized and simultaneously displayed. To construct a power distribution map, we
215 calculated the power of ripple using the periodogram. The period of 10 seconds before SO was
216 defined as the baseline, and the baseline ripple power was obtained from the baseline segment.
217 We calculated the ripple power within a 500-ms sequential time window every 33 ms (30 frame
218 per second). The ripple power ratio was calculated by dividing the ripple power of the 500-ms
219 time window with baseline ripple power. We plotted red circles on the brain image to indicate
220 the electrode locations, and the diameters were scaled linearly with ripple power ratio.

221

222 *2.11. Statistics*

223 The ripple normalized power and SIm values were averaged across all contacts in each
224 seizure, and then averaged ripple normalized power and averaged SIm values were averaged

225 across all seizures. SIm values were normalized using SIm values calculated from the data
226 acquired five minutes before the SO to allow comparison between different low frequency
227 bands. The values greater than +3 standard deviation (SD) or less than -3 SD were excluded as
228 outliers. We used Wilcoxon signed-rank test for pairwise comparison or Wilcoxon rank-sum
229 test for non-pairwise comparison, and Bonferroni correction for multiple comparisons. To
230 compare the ripple power and SIm to the base period (the initial 10-s data), we used a
231 permutation test (Maris and Oostenveld, 2007) and a familywise error (FWE)-corrected
232 threshold for multiple comparisons. Each permutation test produces a set of differences
233 between the base period and the next sequential period. The maximum value of the differences
234 from each permutation test were stored. The values at 95% of the distribution of these
235 maximum values were taken as the FWE-corrected threshold. The values above the FWE-
236 corrected threshold are statistically significant (Cohen, 2014). For comparison of multiple
237 groups, we used the Kruskal-Wallis test.

238 To assess the significant change in SIm, we used the boot-strapping technique. First,
239 the phase of ripple power time series was shifted in time by a random amount. Then, this phase-
240 shifted ripple power time series was used to calculate a SIm value for the purpose of
241 bootstrapping (SImb). For each pair of ripple power and a lower frequency band amplitude,
242 this procedure was repeated 1000 times to create the distribution of SImb (Cohen, 2008). To
243 correct for multiple comparisons, we used the FWE-corrected threshold (95%) (Cohen, 2014).

244

245 *2.12. Data availability*

246 All data that were generated by or analyzed in this study are available from the
247 corresponding authors upon reasonable request and after additional ethics approvals regarding
248 the data provision to individual institutions.

249

250

251 **3. Results**

252

253 *3.1. Profile of ripple power and PAC changes related to seizures*

254 We included seven patients (six male and one female) with 12 focal impaired
255 awareness seizure (FIAS)/FBTCS and three FAS (Table 1). The pathological results of each
256 patient are shown in Table 1. We compared ripple normalized power between the pre-ictal and
257 the ictal states. The ripple normalized power at the ictal state were significantly larger than at
258 the pre-ictal state (single-sided Wilcoxon signed-rank, $P = 3.1 \times 10^{-5}$) (Fig. 2A). Averaged time
259 of seizures is 125.73 ± 55.1 s, and times of each seizure are shown in Table 1. Among all
260 seizures analyzed, SOC were concordant with PRC in 12/15 seizures (80%). When focusing
261 on only FBTCS, SOC matched PRC in all seizures (Table 1).

262 We compared SIm values between ripple activity and each lower frequency band
263 during the burst of ripple power at the ictal state. The normalized SIm of ripple- θ was the
264 highest among all (single-sided Wilcoxon signed-rank with Bonferroni correction, θ - δ :
265 corrected $P = 3.0 \times 10^{-3}$, θ - α : corrected $P = 1.3 \times 10^{-2}$, θ - β : corrected $P = 2.3 \times 10^{-3}$) (Fig. 2B).
266 The main low frequency band coupled with ripple was the δ band in 2/15 seizures (13%), θ
267 band in 12/15 seizures (80%), and α band in 1/15 seizures (7%) (Table 1). We investigated the
268 low frequency power at pre-ictal and ictal states; however, the main low frequency band that
269 showed coupling with ripple did not match the low frequency band showing increased power
270 (Supplementary Fig. 1).

271

272 *3.2. Temporal profile of ripple power and PAC changes*

273 Dynamic changes of ripple normalized power and PAC strength from 5 min before to
274 5 min after the SO are shown in Fig. 2C. A significant burst of ripple power was observed after
275 the SO, which was accompanied by two different profiles of PAC with the lower frequency
276 bands: (1) PAC changes with a peak (θ -, α -, and β -ripple coupling) and (2) PAC changes with

277 a gradual increase and a plateau (δ -ripple coupling). For those with the first profile, the PAC
278 for θ band after SO were the higher than those for α and β bands, which were also reflected in
279 their differences shown in Fig. 2B. For the second profile, the PAC for δ band increased
280 gradually and reached its maximum after ripple power burst, which was not reflected in the
281 difference shown in Fig. 2B that was obtained from the data during the burst of ripple power
282 within the ictal state. We focused on PAC for θ band (representing the first profile) and δ band
283 (the second profile) in the following analyses.

284

285 3.3. Case studies

286 During seizures, the ripple power increased and was coupled with the θ phase. After
287 completion of ripple power burst, δ -ripple coupling occurred. We show the synchronized
288 multimodal data including iEEG waveforms, ripple normalized power, SIm, and ripple power
289 distribution map in the figure and videos of three illustrative cases. In Fig. 3, 4, and 5,
290 significant θ -ripple SIm and representative contacts are shown. In videos (Video 1–3),
291 significant δ - and θ -ripple SIm and all contacts are shown.

292

293 3.3.1 Case #1; Patient 1 (P1)–Seizure 1 (S1)

294 Interictal scalp EEG recorded spike-wave complexes over the right temporal region.
295 We placed intracranial electrodes in the right hemisphere (Fig. 3A). MRI images showed a
296 cystic lesion in the right mesial temporal lobe (MTL) (Fig. 3B).

297 We captured electroclinical seizures consisting of FIAS, followed by FBTCS. Contact
298 A2 on the depth electrode inserted in the right parahippocampal gyrus, showed initial DC shifts,
299 followed by low-voltage fast waves that changed into high-amplitude fast waves and spread to
300 the other electrodes (Fig. 3C). Ripple power increases also began from A2 and spread to the
301 other electrodes (Fig. 3D and 3F). A2 is SOC as well as PRC. Significant θ -ripple SIm values
302 were observed in the contacts in which ripple power increased (Fig. 3E), and after that,

303 significant δ -ripple SIm values were observed (Video 1). Ripple-band power (represented by
304 the size of the red circle) fluctuated rhythmically at certain rhythms when θ -SIm reached
305 statistical significance and this relationship was also observed for δ -band (Video 1).

306 We resected the right mesial temporal lobe including the cystic lesion and the
307 parahippocampal gyrus. Pathological findings showed the presence of dysembryoplastic
308 neuroepithelial tumor. He was seizure-free at the 12-month follow-up.

309

310 3.3.2 Case #2; P4–S2

311 Interictal scalp EEG recorded spike-wave complexes over the left frontotemporal
312 region. We placed intracranial electrodes in the left hemisphere (Fig. 4A). MRI fluid-attenuated
313 inversion recovery (FLAIR) images showed a high-intensity lesion in the left MTL (Fig. 4B).

314 We captured FIAS, followed by FBTCs. Contact A13 on the depth electrodes, which
315 were inserted in the left mesial temporal lesion, showed initial DC shifts, followed by low-
316 voltage fast waves that changed into high-amplitude fast waves and spread to the other
317 electrodes (Fig 4C). Ripple power increases also began from A13 and propagated to other
318 electrodes (Fig. 4D and 4F). A13 is SOC as well as PRC. Significant θ -ripple SIm values were
319 observed in contacts in which ripple power increased (Fig. 4E), and after that, significant δ -
320 ripple SIm values were observed (Video 2).

321 We performed a left selective hippocampectomy including the FLAIR high lesion,
322 also removing the amygdala. Pathological findings showed hippocampal sclerosis. She was
323 seizure-free at the 12-month follow-up.

324

325 3.3.3. Case #3; P5–S2

326 Interictal scalp EEG recorded spike-wave complexes over the right temporo-occipital
327 region. We placed intracranial electrodes in the right hemisphere (Fig. 5A). MRI FLAIR images
328 showed a high-intensity lesion in the right occipital lobe (Fig. 5B).

329 We captured electroclinical seizures, followed by bilateral lower extremities
330 stereotypies (FBTCS). The A31, A32, A36 and A37 contacts, which were placed over the
331 occipital lesion, showed initial DC shifts, followed by low-voltage fast waves that changed into
332 high-amplitude fast waves (Fig. 1A, Fig. 5C). Ripple power increases also began from these
333 four contacts and propagated to the other electrodes (Fig. 5D and 5F). SOC-PRC concordance
334 was observed. Significant θ -ripple SIm values started to appear in contacts which were placed
335 over the occipital lesion (Fig. 5E), and after that, significant δ -ripple SIm values were also
336 observed (Video 3).

337 We performed a resection surgery of the right occipital lesion. Pathological findings
338 showed diffuse glioma. He was seizure-free at the 12-month follow-up.

339

340 In all three cases, SOC was concordant with the PRC, and the time lag between θ and
341 δ PAC was observed. Rhythmically fluctuations of ripple activities were visualized in the
342 power distribution map when the values of SIm were significantly high (Video 1, 2, and 3).

343

344 *3.4. Time when the maximum values were observed*

345 There was no significant difference between the time taken (since SO) to attain
346 maximum ripple power (77.6 ± 38.9 s) and maximum θ PAC (73.7 ± 41.7 s); however, the time
347 taken to achieve maximum value of δ PAC (117.7 ± 70.9 s) was significantly more than that
348 for both ripple power and θ PAC (single-sided Wilcoxon signed-rank with Bonferroni
349 correction, ripple power and δ PAC, corrected $P = 1.6 \times 10^{-3}$, θ PAC and δ PAC, corrected $P =$
350 8.2×10^{-4}) (Fig. 6A). A time lag between θ and δ PAC was observed in 14/15 seizures (93.3%)
351 (Table 1).

352

353 *3.5. Correlation between ripple normalized power and SIm*

354 To clarify the differences between PAC for θ and δ bands, correlation analysis was

355 used. The correlation of ripple with the SIm of θ band was positive in all three states (pre-ictal,
356 ictal and late-ictal), in which a statistical significance was reached in the ictal state. In contrast,
357 the correlation with the SIm of δ band was positive in the pre- and late-ictal states and negative
358 in the ictal state, in which a statistical significance was reached in all three states (Fig. 6B).

359

360 *3.6. Phase-tuning ripple power*

361 The oscillation of δ and θ bands showed a trough at 180° in all pre-ictal, ictal and
362 late-ictal states (Fig. 6C). In the ictal state, in which θ -SIm increased (Fig. 2C), ripple
363 normalized power peaked at the trough of the θ oscillation but not the δ oscillation (Fig. 6C).
364 In the late-ictal state, in which δ -SIm increased (Fig. 2C), ripple normalized power peaked at
365 the trough of the δ oscillation (Fig. 6C).

366

367 *3.7. Comparison between FBTCS and FAS*

368 In 12 FBTCS in which seizures showed sequential changes from no motor symptom
369 to tonic seizures and finally to clonic seizures, the average dynamic changes in the ripple
370 normalized power were compared at these different ictal phases (Fig. 7A). The ripple
371 normalized power of both tonic and clonic phases was significantly higher than that of the no
372 motor symptom phase; however, there were no significant changes between the tonic and clonic
373 phases (both-sided Wilcoxon rank-sum with Bonferroni correction, no motor-tonic: corrected
374 $P = 1.9 \times 10^{-116}$, tonic-clonic: corrected $P = 1.2$, no motor-clonic: corrected $P = 2.7 \times 10^{-110}$).

375 Finally, we compared θ -ripple SIm and ripple normalized power acquired from the
376 SOC during the no motor symptom phase between FBTCS and FAS (Fig. 7B). FBTCS showed
377 significantly higher values than FAS in SIm (both-sided Wilcoxon rank-sum, $P = 2.3 \times 10^{-267}$)
378 and ripple normalized power (both-sided Wilcoxon rank-sum, $P = 0$).

379

380 **4. Discussion**

381 This study demonstrated that a ripple power burst occurs during seizures, and the
382 phase of θ band modulates ripple power involved in seizures. Our videos showed that when
383 ripple power increased, the individual ripple power of each contact (corresponded to the size
384 of each red circle in the video) changes rhythmically. During such rhythmic fluctuation in the
385 circles' size, a significant θ -ripple PAC was observed. Therefore, we inferred that the rhythmic
386 fluctuation in the circles' size (in the video) was modulated by the θ rhythm and this fluctuation
387 represented the θ -ripple PAC phenomenon. Our video also showed that in FBTCS, ripple
388 activities involved in seizures started to increase from the focal area and spread to other regions,
389 but with fluctuations and not linearly.

390

391 How HFAs were propagated during seizures has been visualized by topographic
392 videos (Akiyama et al., 2011, Akiyama et al., 2006), however, PAC changes involved in
393 seizures have not been visualized. In our videos, the diameters of each circle that represents an
394 implanted electrode contact changed with ripple power, and the videos also demonstrated the
395 propagation of HFAs by dynamic changes of circles' diameters. Moreover, the rhythmic
396 fluctuations of the diameter were observed in each contact. When δ - or θ -ripple PAC
397 significantly increased, the rhythmic fluctuation of the circles' diameter became especially
398 obvious. We inferred that this rhythmic fluctuation of the circles' diameter was tuned at δ - or θ
399 rhythm, and concluded that this rhythmic fluctuation visualized the PAC phenomenon.

400

401 HFAs have been observed during seizures (Akiyama et al., 2011, Ochi et al., 2007)
402 and HFOs are suggested as useful biomarkers for detection of the SOZ (Wang et al., 2013, Wu
403 et al., 2014). In this study, significant increase in ripple power was observed during seizures,
404 and PRC which showed preceding ripple activities were demonstrated (Fig. 3D, 4D, and 5D,
405 and videos). The SOC was conventionally determined by visual inspection (Perucca et al.,
406 2014), and we demonstrated that in FBTCS, the SOCs were concordant with the PRCs.

407 Therefore, we thought that ripple activities were useful for detection of the SOZ.

408

409 In FBTCS, the more the seizure progressed, the more the ripple activities increased.
410 The videos in this study showing seizure evolution of FBTCS demonstrated that the focal
411 fluctuations of ripple activities increased and spread to other regions. The results of the videos
412 indicated that ripple activities involved in seizures increased and spread with fluctuations, but
413 not linearly. In clinical situations, our video helped us find the SOZ using focal ripple activities.
414 Moreover, in actual clinical settings, we synchronized the multimodal data (iEEG, ripple
415 normalized power, and SIm) with video images captured by the video-EEG camera; therefore,
416 we could infer the symptomatogenic zone by correlating seizure symptoms captured by video-
417 EEG camera with the spread of ripple activities. In this study, images captured by the video-
418 EEG camera were not presented because of privacy issues.

419

420 In line with a previous study (Ibrahim et al., 2014), our study demonstrated that θ band
421 was the main low frequency band modulating ictal-ripple activities and α - and β -ripple PAC
422 showed the same tendency as the θ -ripple PAC with a weaker PAC though. Moreover, it is
423 reported that coupling with θ waves and HFOs well discriminated normal brain regions from
424 SOZ (Amiri et al., 2019). Therefore, we inferred that ripple activities occurring during early
425 seizure evolution were modulated by θ rhythm. The occurrence of maximal ripple power at the
426 trough of the low frequency oscillation was concordant with a previous study (Ibrahim et al.,
427 2014). In an interictal state, a positive correlation between coupling and ripple amplitude were
428 known (Weiss et al., 2016), and we showed the positive correlation between θ -ripple PAC and
429 ripple power during the ictal state.

430

431 Previous studies showed that prior to the onset of bilateral tonic-clonic movements,
432 ripple density in the SOZ was higher in FBTCS than in focal seizures (Schönberger et al., 2019).

433 This result is concordant with our result that in the SOZ, the ripple normalized power was
434 higher in FBTCS than in FAS during the early no motor symptom phase. Moreover, we showed
435 that θ -ripple SIm was also higher in FBTCS than in FAS, which reflected the results of the
436 positive correlation between θ -ripple PAC and ripple power during the ictal state.

437

438 The low frequency band that coupled with ripple activities involved in seizures varied
439 in one patient and also between patients; however, in most seizures, the θ band is the main band.
440 Between various pathological results, the main low frequency coupling with ripple activities
441 was the θ band in common. This result might indicate the common neurophysiological
442 processing that neural activities involved in seizure generation and spreading were mainly
443 regulated by the θ rhythm. Animal experiments showed that in the epileptic brain, the
444 hippocampal θ rhythm was increased (Kitchigina and Butuzova, 2009). However, in this study,
445 the sample size was too small to investigate the statistical differences or similarities of each
446 pathology.

447

448 A seizure is generated by depolarization and repetitive firing of neurons, and the
449 frequency of epileptic EEG activities have been shown to be involved in the thalamocortical
450 network (Dichter, 1997). HFA power is strongly correlated with neural firing rate (Ray et al.,
451 2008), and in animal studies, neural spiking is locked to the trough of the α oscillations
452 (Haegens et al., 2011). Our results showed that ripple normalized power peaked at the trough
453 of the δ or θ oscillation during coupling occurrences. This result may indicate that repetitive
454 neural firing involve in seizure generation is locked to the trough of the δ or θ oscillations.
455 Furthermore, the neural mechanism for how tonic and clonic seizures are induced in FBTCSs
456 has remained unclear. In all FBTCSs of this study, we observed a time lag between the first
457 occurrence of a θ -ripple coupling and the next occurrence of a δ -ripple coupling. Since a tonic
458 seizure occurred first and then a clonic seizure occurred next in FBTCSs, we hypothesized the

459 following neurophysiological mechanism in FBTCs: the thalamus first modulates the cortex
460 at the θ rhythm and then a tonic seizure is induced; next, the thalamus modulates the cortex at
461 the δ rhythm and then a clonic seizure is induced.

462

463 We showed finding that δ -ripple PAC had a negative correlation with ripple power
464 during ictal-ripple power burst, and increased after ictal-ripple power burst subsided. Coupling
465 between HFAs and δ band were investigated in previous studies associated with epileptic
466 spasm(Nariai et al., 2011) and an interictal state(Amiri et al., 2016). Our videos brought a new
467 insight that δ -ripple PAC significantly increased after θ -ripple PAC. Our results suggested that
468 δ - and θ -ripple PAC were caused by different mechanisms, and this explained the time lag
469 between δ - and θ -ripple PAC.

470

471 This study had some limitations. Because intracranial EEG electrodes covers only a
472 small portion of the brain, we can never be sure if the intracranial electrodes were placed in the
473 actual SOZ, and thus the activities that we analyzed may not be the actual activities from the
474 SOZ. To limit the effect of this uncertainty, we used the average ripple power and SIm from all
475 electrodes because we could evaluate at least seizure-related changes which were propagated
476 activities from the SOZ not focal activities of the SOZ. All the seizures were recorded after an
477 extensive reduction of antiepileptic drugs, and thus, they might not represent the patients' usual
478 seizures. However, our analysis were independent from this issue because reduction in
479 medication does not affect the morphology of discharges at onset, and duration of contralateral
480 spread (So and Gotman, 1990). Because this study included only patients with focal epilepsy,
481 our findings may not be generalized to patients with generalized epilepsy. Moreover, because
482 we had only three seizures of FAS, more FAS cases must be analyzed to confirm the differences
483 between FBTCs and FAS. Finally, our sampling rate of iEEG was 1 kHz; therefore, the
484 available frequency range was limited under 300 Hz, and fast ripples usually corresponding to

485 250-500/600 Hz could not be analyzed.

486

487

488 **5. Conclusions**

489 By analyzing seizure evolution of focal epilepsy using ripple power and PAC, this
490 study revealed that θ band is the main low frequency band modulating ripple power during
491 ictal-ripple burst. The video we created demonstrated that ripple powers began to increase
492 focally with fluctuations, and spread with fluctuations, not with linear increases. We concluded
493 that the fluctuations are a visualization of the PAC phenomenon. The θ oscillations might
494 represent the common neurophysiological processing involved in seizure generation.

495

Preprint

496 **Declaration of Competing Interest**

497 The authors declare that they have no known competing financial interests or personal
498 relationships that could have appeared to influence the work reported in this paper.

499

500 **Acknowledgements**

501 This study was supported by the Grants-in-Aid for Scientific Research (A) (KAKENHI; grant
502 no., 18H04166) and the Grants-in-Aid for Early-Career Scientists (KAKENHI; grant no.,
503 18K18366), which are funded by the Japan Society for the Promotion of Science (JSPS; Tokyo,
504 Japan).

505

506 **Author Contributions**

507 H.H. conceived the study, collected the data, created the MATLAB program, analyzed the data,
508 created all figures and the video, and was primarily responsible for writing the manuscript.
509 H.M.K., N.T., S.O., H.K., and M.H. performed the epileptic surgery. All authors clinically
510 cared for and evaluated the patient. H.M.K., T.Y., and M.H. advised H.H. on scientific matters.
511 H.M.K revised the manuscript. H.K. and M.H. supervised this study. All authors have reviewed
512 the manuscript.

513

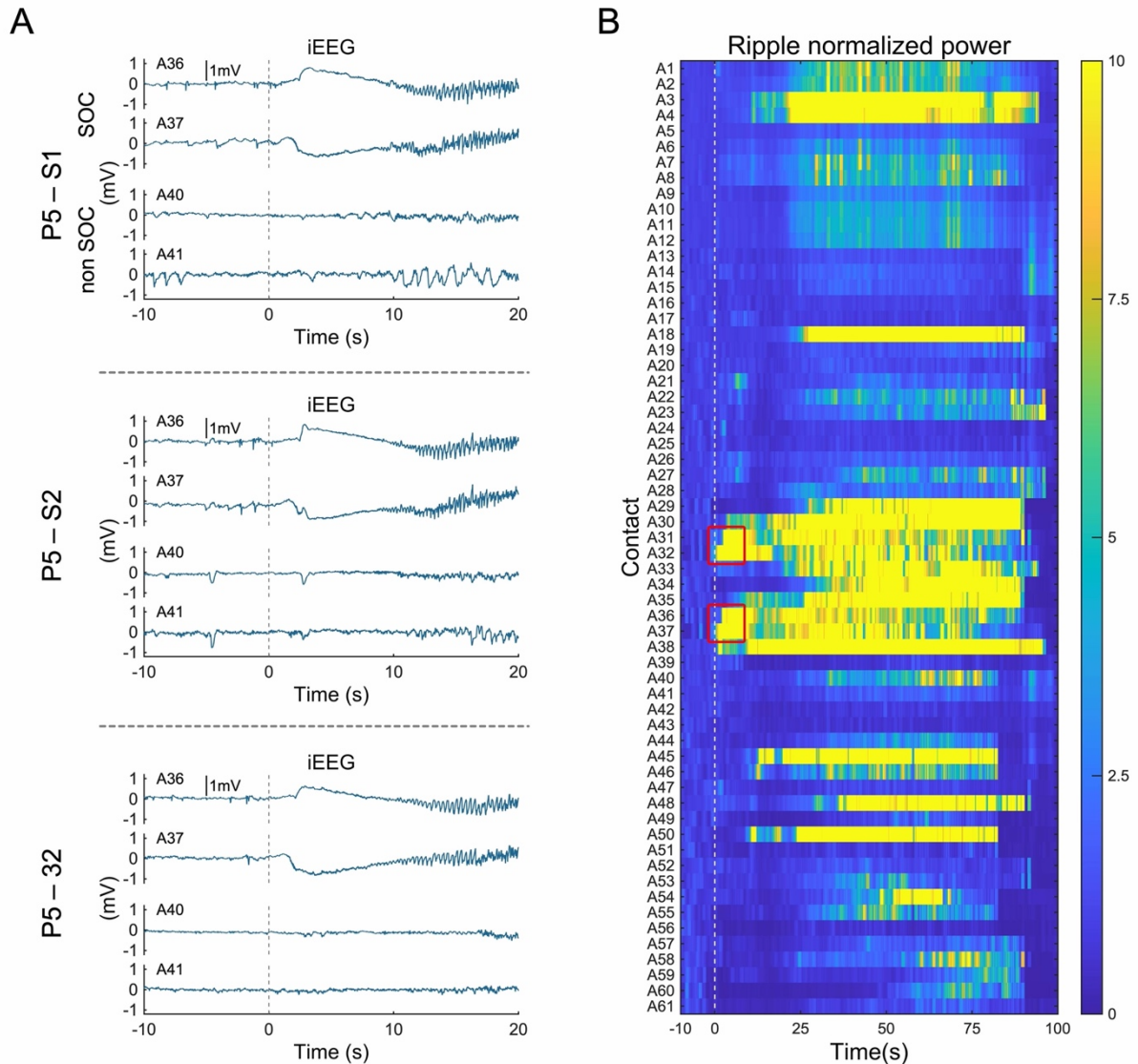
Patients number	Sex	Laterality	Pathology	Seizure numbers	Seizure type	Seizure duration (s)	Preceding ripple activities	SOC-PRC concordance	Coupling low frequency band	Time lag between δ and θ coupling
P1	Male	Right	MTLE DNT	S1	FIAS→FBTCS	154	Yes	concordant	θ	Yes
				S2	FIAS→FBTCS	144	Yes	concordant	θ	Yes
				S3	FIAS→FBTCS	156	Yes	concordant	α	Yes
				S4	FIAS→FBTCS	266	Yes	concordant	θ	Yes
				S5	FIAS→FBTCS	184	Yes	concordant	θ	Yes
P2	Male	Right	PLE Glial-cortical tissue with psammoma body-like lesion	S1	FIAS→FBTCS	49	Yes	concordant	δ	Yes
P3	Male	Left	OLE*	S1	FIAS→FBTCS	132	Yes	concordant	θ	Yes
P4	Female	Left	MTLE, HS	S1	FIAS→FBTCS	102	Yes	concordant	θ	Yes

				S2	FIAS→FBTCS	113	Yes	concordant	θ	Yes
P5	Male	Right	OLE Diffuse glioma	S1	FIAS→FBTCS	96	Yes	concordant	θ	Yes
				S2	FIAS→FBTCS	81	Yes	concordant	θ	Yes
				S3	FIAS→FBTCS	129	Yes	concordant	θ	Yes
P6	Male	Left	MTLE HS	S1	FAS	149	Yes	discordant	θ	No
P7	Male	Right	MTLE FCD	S1	FAS	67	Yes	discordant	θ	Yes
				S2	FAS	64	Yes	discordant	δ	Yes

Table 1 Clinical profile.

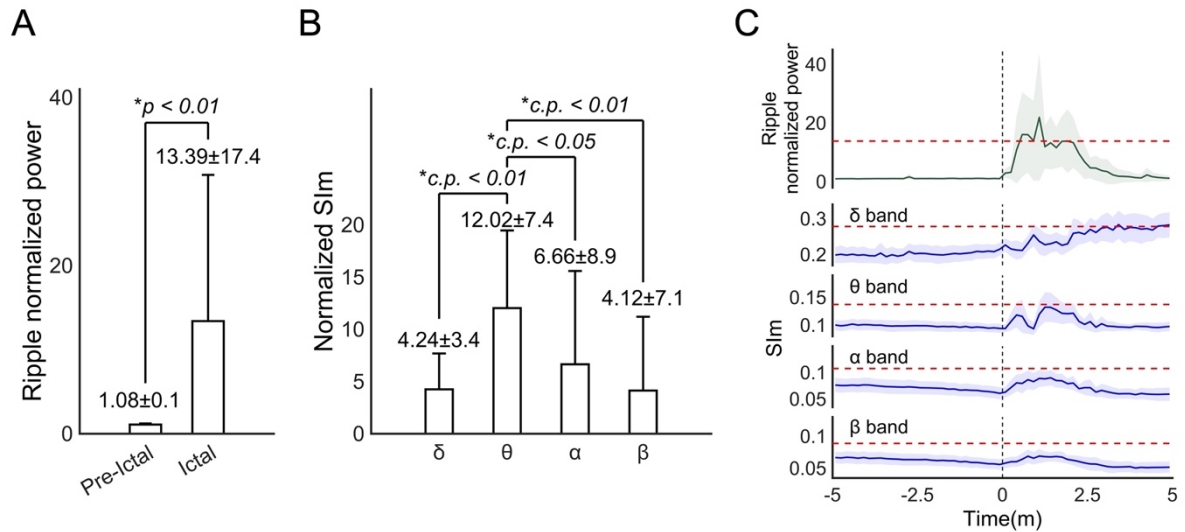
DNT, Dysembryoplastic neuroepithelial tumor; FAS, Focal aware seizure; FBTCS, Focal to bilateral tonic-clonic seizure; FCD, Focal cortical dysplasia; FIAS, Focal impaired awareness seizure; HFAs, High-frequency activities; HS, Hippocampal sclerosis; MTLE, Mesial temporal lobe epilepsy; OLE, Occipital lobe epilepsy; PLE, Parietal lobe epilepsy; PRC, Preceding ripple contact; SOC, Seizure onset contact;

*Focal resection surgery had not been performed because the detection of the seizure onset zone was impossible.



514
 515
 516
 517
 518
 519
 520
 521
 522
 523
 524
 525
 526
 527
 528

Figure 1 Seizure onset contact (SOC) and preceding ripple contact (PRC)
 Patient 5 (P5) showed three focal-to-bilateral tonic-clonic seizures (Seizure 1(S1), S2 and S3).
 A. Initial raw intracranial electroencephalogram (iEEG) changes included disappearance of background activities, DC shifts, and low-voltage fast waves. The contact of A31, A32, A36, and A37 (only A36 and A37 are displayed) showed the same pattern of epileptic discharges across all three seizures. We defined these four contacts as SOC, and we randomly selected one contact—A36 in this patient—for further investigations. For reference, the non SOC, A40 and A41 that showed no epileptic changes at the seizure onset (SO) were displayed. B. Ripple normalized powers are shown. Immediately after the SO, ripple normalized powers >10 were observed a cluster at A31, A32, A36, and A37 (red square). These ripple activities preceded the later ripple activities by several seconds, and we defined them as *preceding ripple activities*. Therefore, above four contacts were the PRC, and the SOC matched the PRC in P5. The 0 s corresponded to the SO. All implanted contacts are indicated on the vertical axis of B.



529

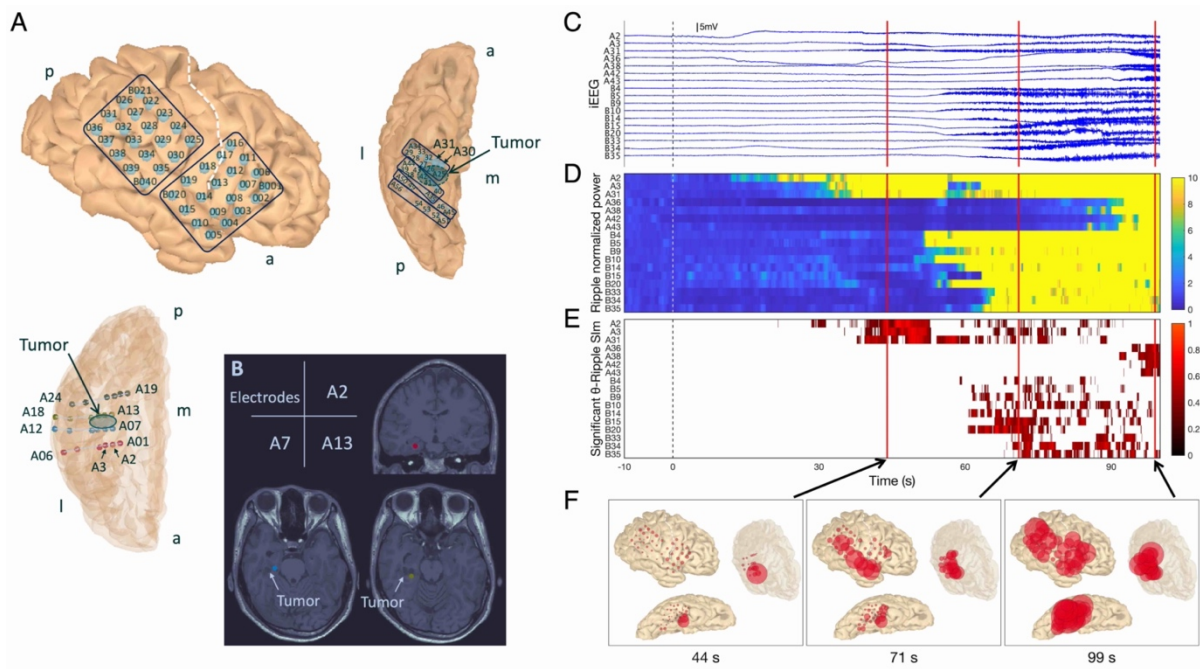
530 **Figure 2** Characteristics of ripple power and phase-amplitude coupling (PAC) related to
 531 seizures.

532 A. The ripple normalized power in ictal state was significantly greater than that in pre-ictal
 533 state. B. The normalized synchronization index magnitude (SIm) during ripple power burst
 534 related to seizures achieved the significant highest values in θ band. C. Temporal plot of ripple
 535 normalized power, θ -, α -, and β -SIm increased and achieved the peak after the seizure onset
 536 (SO) (0 min). δ -SIm achieved the peak after completion of ripple power burst. The familywise
 537 error (FWE)-corrected threshold is indicated as red dashed line.

538 c.p: corrected p value with Bonferroni correction. The error bars (EB) in A, and B indicate
 539 standard deviation. The EB in C indicate 95% confidence intervals.

540

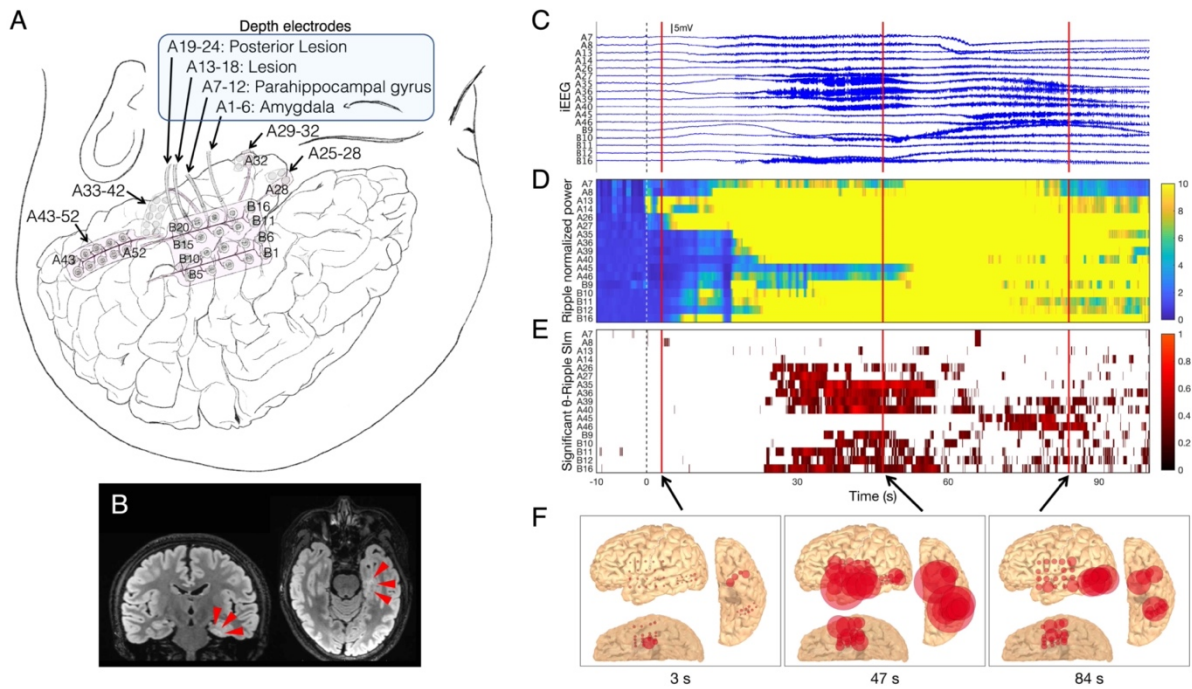
541



542
 543
 544
 545
 546
 547
 548
 549
 550
 551
 552
 553
 554
 555
 556
 557
 558

Figure 3 Seizure profile in Patient 1 (P1)-Seizure 1 (S1).

A. Depth electrodes A1–6, A7–12, A13–18, and A19–24 were targeting the parahippocampal gyrus, the anterior region of the tumor, the posterior region of the tumor, and the lingual gyrus, respectively. a. anterior; p. posterior; m. medial; l. lateral. B. The location of A2, A7, and A13 in relation the cystic tumor is shown on the T1-weighted magnetic resonance imaging. C. Intracranial electrodes’ raw signals. Initial infraslow activities were observed on A2. D. The ripple normalized power started to increase after the seizure onset (SO), from the A2 and propagated to other contacts. E. Significant θ -ripple synchronization index magnitude (Sim) shows the cluster in contacts in which ripple power increased. Here, 0 s corresponds to the SO determined visually and is indicated as dashed lines. F. Ripple power distribution map. The location of red circles corresponds to each contact’s location, and those located within the semitransparent brain were depth electrode contacts. The size of red circles corresponds to ripple power. The ripple power started to increase in A2 (44 s) and propagated to other contacts on the cortex along the Sylvian fissure (71 s), and almost all other regions (99 s).



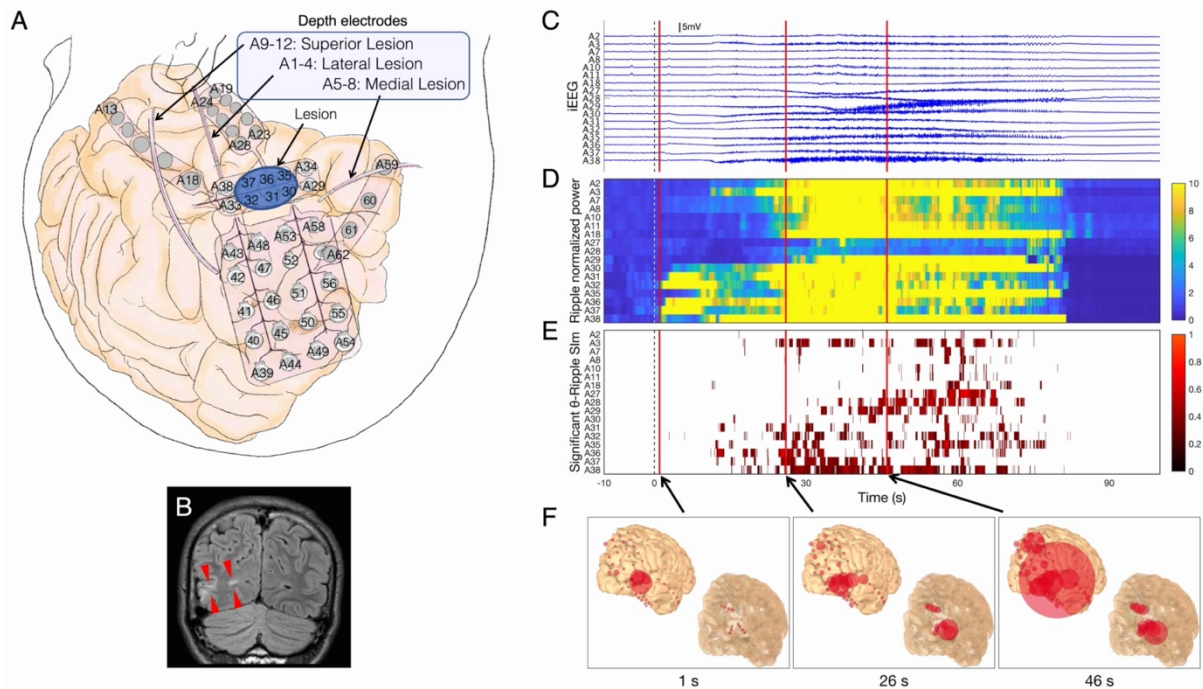
559

560 **Figure 4** Seizure profile in Patient 4 (P4)-Seizure 2 (S2).

561 A. Depth electrodes A1–24 were inserted into the left mesial temporal lobe (MTL). A13 was
 562 located in the lesion. B. The high-intensity lesion in the left MTL is shown on fluid-attenuated
 563 inversion recovery magnetic resonance imaging (red wedge arrows). C. In A13, initial
 564 infraslow activities and low-voltage fast waves were observed. D. The ripple normalized power
 565 started to increase after the seizure onset (SO), from A13 and propagated to other contacts. E.
 566 Significant θ -ripple synchronization index magnitude (SIm) shows the cluster in contacts in
 567 which ripple power increased. Here, 0 s corresponds to the SO determined visually and is
 568 indicated as dashed lines. F. Ripple power distribution map. The location of red circles
 569 corresponds to each contact’s location, and those located within the semitransparent brain were
 570 depth electrode contacts. The size of red circles corresponds to ripple power. The ripple power
 571 started to increase in A13 (3 s) and propagated to other contacts on the cortex along the Sylvian
 572 fissure (47 s), and to the posterior middle temporal gyrus (84 s).

573

574



575

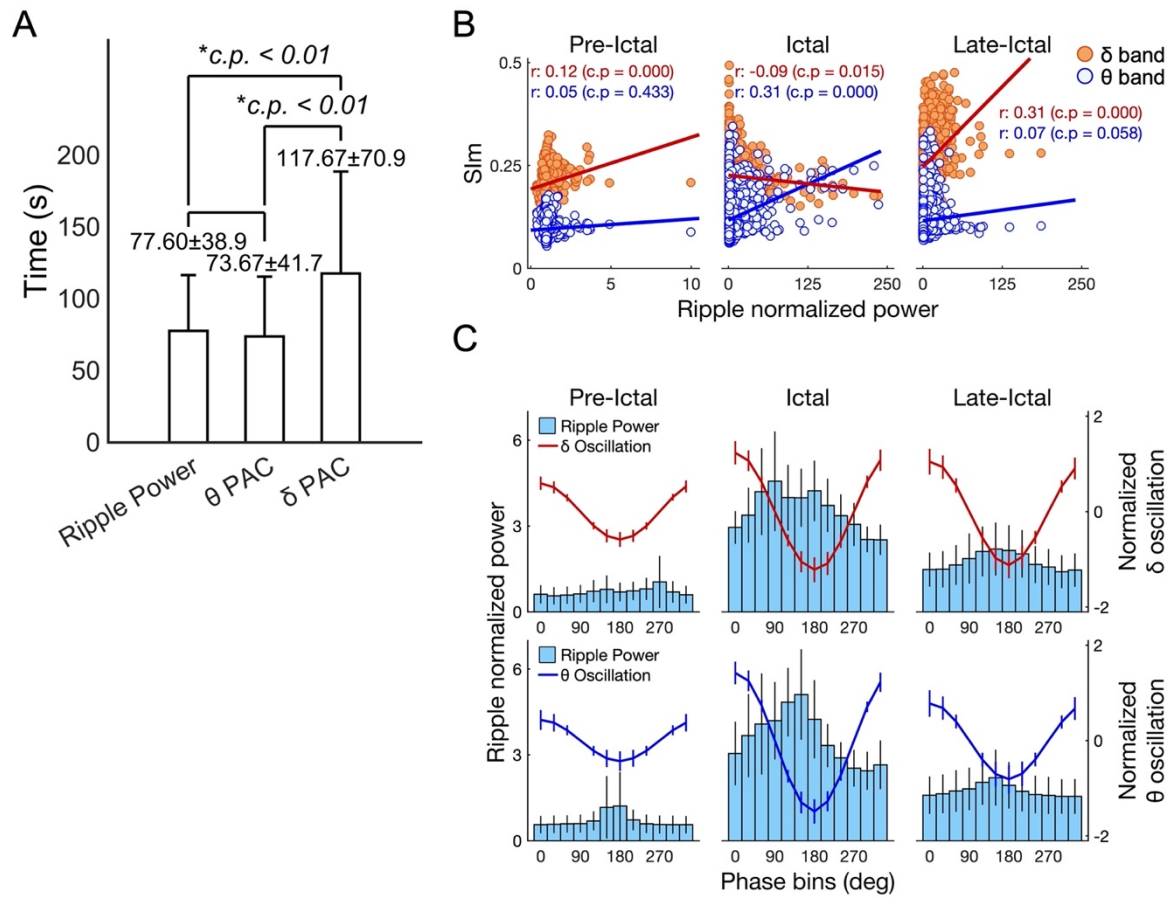
576 **Figure 5** Seizure profile in Patient 5 (P5)-Seizure 2 (S2).

577 A. Depth electrodes A1–12 were targeting around the right occipital lesion. B. The high-
 578 intensity lesion in the right occipital lobe is shown on fluid-attenuated inversion recovery
 579 magnetic resonance imaging (red wedge arrows). C. In A31, A32, A36 and A37, initial
 580 infraslow activities and low-voltage fast waves were observed. D. The ripple normalized
 581 power started to increase after the seizure onset (SO), from the A31, A32, A36 and A37 and
 582 propagated to other electrodes. E. Significant θ -ripple synchronization index magnitude
 583 (SIm) shows the cluster in contacts in which ripple power increased. Here, 0 s corresponds to
 584 the SO determined visually and is indicated as dashed lines. F. Ripple power distribution
 585 map. The location of red circles corresponds to each contact's location, and those located
 586 within the semitransparent brain were depth electrode contacts. The size of red circles
 587 corresponds to ripple power. The ripple power started to increase in A31, A36 and A37
 588 over the right occipital lesion (1 s) and propagated to the parietal lobe (46 s).

589

590

591



592

593 **Figure 6** Characteristics of δ - and θ -ripple phase-amplitude coupling (PAC) related to seizures.

594 A. The time taken to achieve the maximum values was compared between ripple normalized

595 power, θ -SIm (PAC), and δ -SIm (PAC). The time of δ PAC was significantly slower. B. During

596 ictal state, significant positive correlation between ripple normalized power and θ -SIm and

597 significant negative correlation between ripple normalized power and δ -SIm were observed. In

598 late-ictal state, significant positive correlation between ripple normalized power and δ -SIm was

599 observed. r: correlation coefficients, c.p: corrected p value with Bonferroni correction. C. Phase

600 tuning δ and θ oscillation showed the trough at 180° . The phase-tuning ripple normalized power

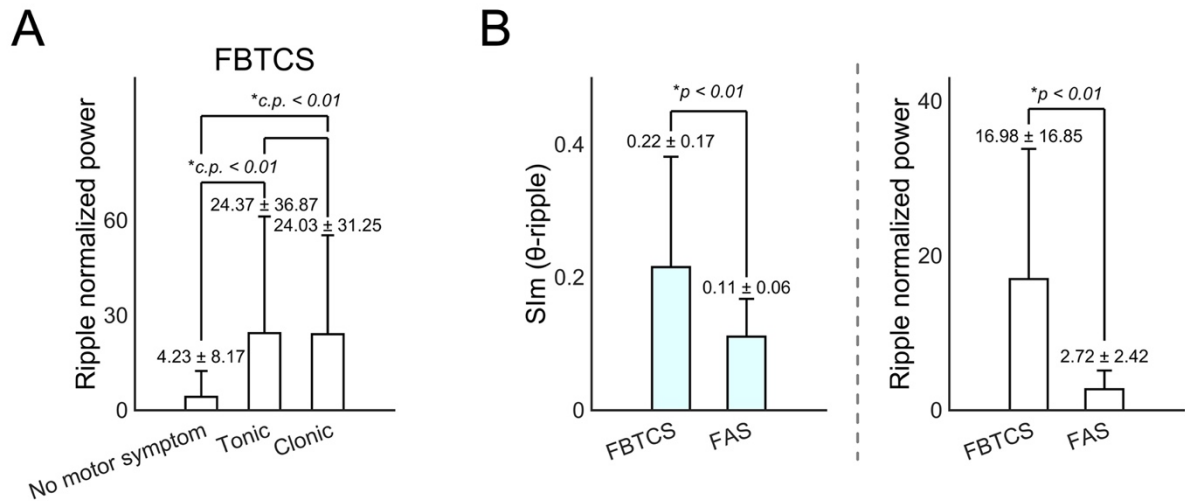
601 showed the peak at the trough with θ phase in ictal state, and with δ phase in late-ictal state.

602 The error bars (EB) in A indicate standard deviation. The EB in C indicate 95% confidence

603 intervals.

604

605

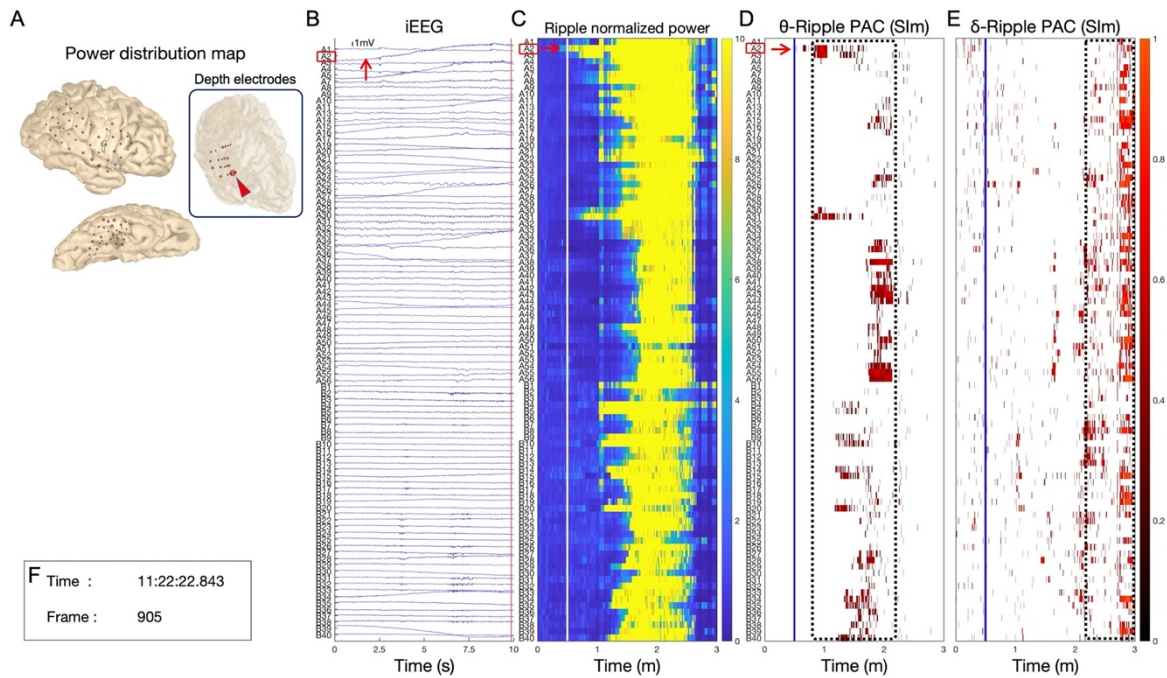


606
607
608
609
610
611
612
613
614
615
616
617

Figure 7 Profile of focal to bilateral tonic clonic seizure (FBTCS) and focal aware seizure (FAS).

A. In FBTCS, the seizure phase changed from the no motor symptom phase, to tonic phase, and then to the clonic phase. Both the tonic and clonic phases showed significantly higher ripple normalized power—averaged from all contacts—than the no motor symptom phase. B. θ -ripple SIm and ripple normalized power obtained from seizure onset contact were compared during the no motor symptom phase between FBTCS and FAS. FBTCS showed significantly higher SIm and ripple normalized power than FAS.

c.p.: corrected p value with Bonferroni correction.



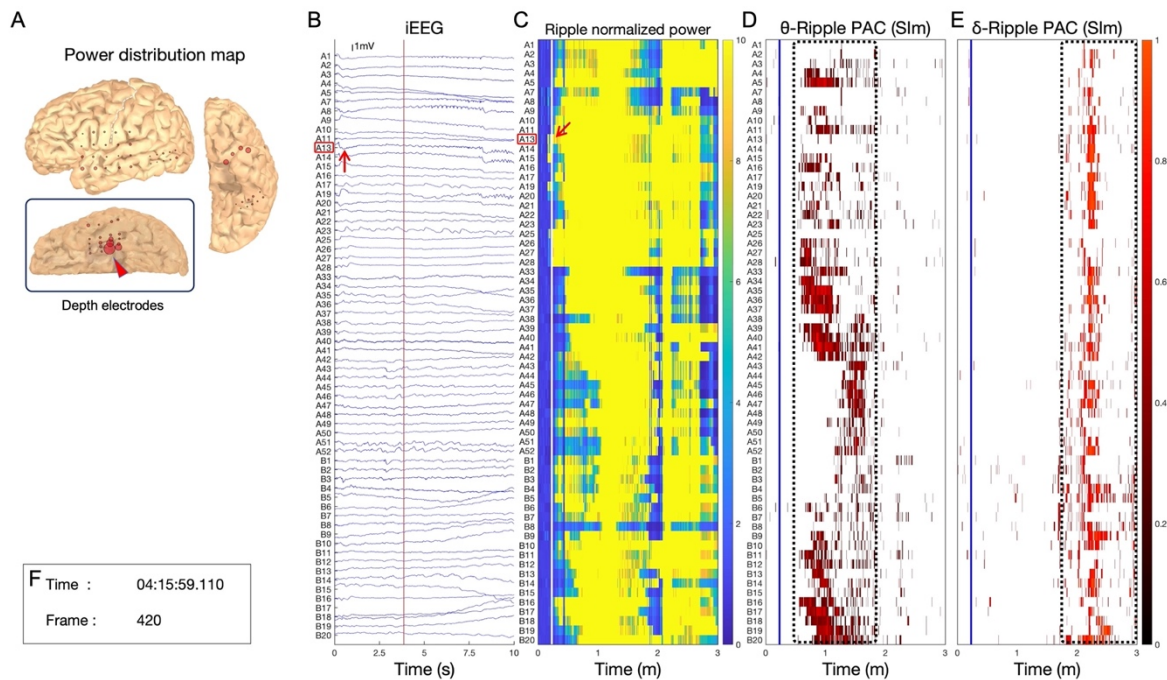
618

619 **Video 1**

620 Multimodal data obtained from Patient 1-Seizure 1 are shown; ripple (80–250 Hz) power
 621 distribution map (A), intracranial electroencephalograms (iEEG) signals (B), ripple normalized
 622 power (C), θ -ripple phase-amplitude coupling (PAC) (synchronization index magnitude: SI_m)
 623 (D), δ -ripple PAC (SI_m) (E) and time (F). The video starts 10 s before the seizure onset (SO).
 624 In power distribution map (A), red circles, corresponding to intracranial electrode contacts,
 625 were scaled linearly with ripple power changes. The circles in the semitransparent brain
 626 indicate depth electrode contacts. The rhythmic movement of red circles started from the A2
 627 depth electrode contact (red wedge arrow), which were inserted into the right parahippocampal
 628 gyrus (A). The rhythmic fluctuations spread to the contacts over the cortex along the Sylvian
 629 fissure and that over the temporal base. The A2 contact showed initial infraslow activities (red
 630 arrow in B), followed by low-voltage fast waves, therefore we defined the A2 contact as a
 631 seizure onset contact (SOC). Ripple power increases also began from the A2 (red arrow in C),
 632 therefore in this case, a preceding ripple contact (PRC) was the A2 contact and the SOC was
 633 concordant with the PRC. SI_m values scaled as black to red are statistically significant values
 634 to which the FWE-corrected threshold was applied. At ripple power increasing from the A2
 635 contact, significant θ -ripple PAC were also observed (red arrow in D). First, significant θ -ripple
 636 PAC were observed (black dashed square in D), after that, significant δ -ripple PAC were
 637 observed (black dashed square in E). In this case, time lag between θ - and δ -ripple PAC were
 638 observed. During significantly high values of SI_m, the fluctuation of red circles changed at
 639 certain rhythms. We inferred that the rhythmic fluctuations were tuned at θ or δ rhythm, and
 640 represented the PAC phenomenon. The SO is 11:22:03. The 44 s, 71 s, and 99 s in Fig. 3F
 641 correspond to 11:22:47, 11:23:14, and 11:23:42 in respectively. All implanted electrode

642 contacts after removal of noisy contacts are shown in the vertical axes (B, C, D, and E). The
643 vertical bars indicating current-time are colored red in iEEG signals (B), white in ripple
644 normalized power (C), and blue in PAC (D, and E). The vide was played at 1.5x.
645

Preprint



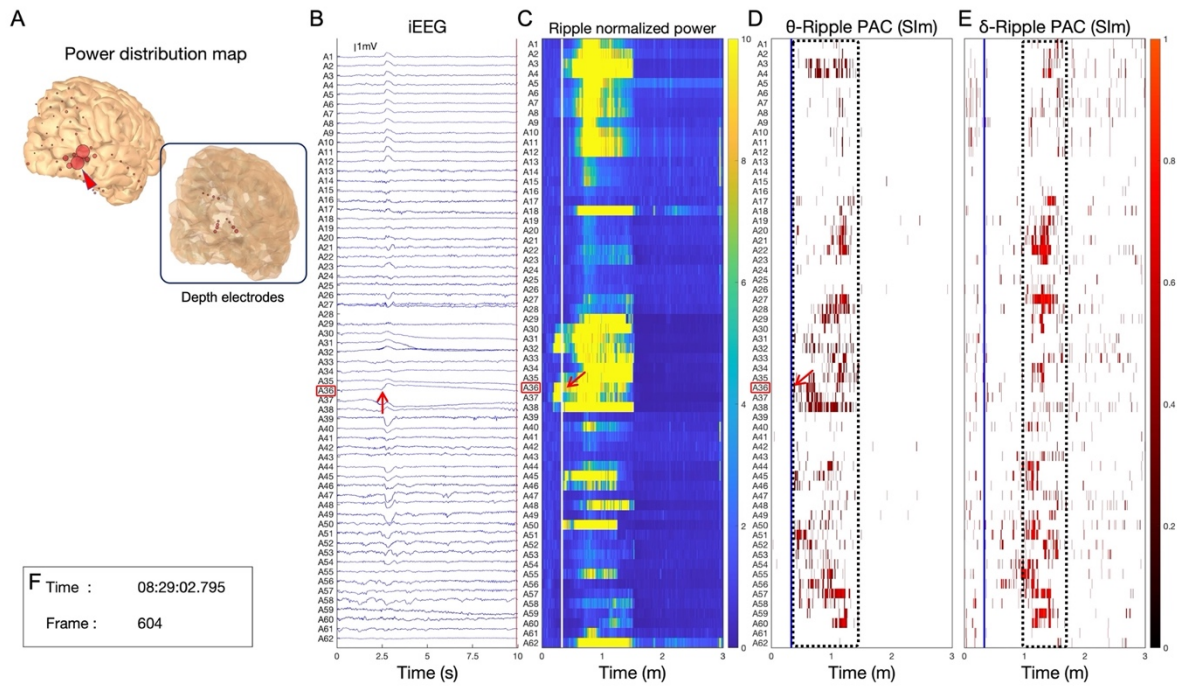
646

647 **Video 2**

648 Multimodal data obtained from Patient 4-Seizure 2 are shown; ripple (80–250 Hz) power
 649 distribution map (A), intracranial electroencephalograms (iEEG) signals (B), ripple normalized
 650 power (C), θ -ripple phase-amplitude coupling (PAC) (synchronization index magnitude: SI_m)
 651 (D), δ -ripple PAC (SI_m) (E) and time (F). The video starts 10 s before the seizure onset (SO).
 652 In power distribution map (A), red circles, corresponding to intracranial electrode contacts,
 653 were scaled linearly with ripple power changes. The circles in the semitransparent brain
 654 indicate depth electrode contacts. The rhythmic movement of red circles started from the A13
 655 depth electrode contact (red wedge arrow), which were inserted into the left mesial temporal
 656 lobe (A). The rhythmic movement spread to the contacts over the temporal tip cortex and that
 657 over the cortex along the Sylvian fissure and that over the posterior middle temporal gyrus.
 658 The A13 contact showed initial infraslow activities (red arrow in B), followed by low-voltage
 659 fast waves, therefore we defined the A13 contact as a seizure onset contact (SOC). Ripple
 660 power increases also began from the A13 (red arrow in C), therefore in this case, a preceding
 661 ripple contact (PRC) was the A13 contact and the SOC was concordant with the PRC. SI_m
 662 values scaled as black to red are statistically significant values to which the FWE-corrected
 663 threshold was applied. First, significant θ -ripple PAC were observed (black bashed square in
 664 D), after that, significant δ -ripple PAC were observed (black bashed square in E). In this case,
 665 time lag between θ - and δ -ripple PAC were observed. During significantly high values of SI_m,
 666 the fluctuation of red circles changed at certain rhythms. We inferred that the rhythmic
 667 fluctuations were tuned at θ or δ rhythm, and represented the PAC phenomenon. The SO is
 668 4:15:56. The 3 s, 47 s, and 84 s in Fig. 4F correspond to 4:15:59, 4:16:43, and 4:17:20 in
 669 respectively. All implanted electrode contacts after removal of noisy contacts are shown in the

670 vertical axes (B, C, D, and E). The vertical bars indicating current-time are colored red in iEEG
671 signals (B), white in ripple normalized power (C), and blue in PAC (D, and E). The vide was
672 played at 1.5x.
673

Preprint



674

675 **Video 3**

676 Multimodal data obtained from Patient 5-Seizure 2 are shown; ripple (80–250 Hz) power
 677 distribution map (A), intracranial electroencephalograms (iEEG) signals (B), ripple normalized
 678 power (C), θ -ripple phase-amplitude coupling (PAC) (synchronization index magnitude: SI_m)
 679 (D), δ -ripple PAC (SI_m) (E) and time (F). The video starts 10 s before the seizure onset (SO).
 680 In power distribution map (A), red circles, corresponding to intracranial electrode contacts,
 681 were scaled linearly with ripple power changes. The circles in the semitransparent brain
 682 indicate depth electrode contacts. The rhythmic movement of red circles started from the
 683 surface electrode contacts which were placed over the right occipital lesion, including the A36
 684 contact (red wedge arrow in A). The rhythmic movement spread to the contacts over the parietal
 685 lobe. The A36 contact showed initial infraslow activities (red arrow in B), followed by low-
 686 voltage fast waves, therefore we defined the A36 contact as a seizure onset contact (SOC).
 687 Ripple power increases also began from the A36 (red arrow in C), therefore in this case, a
 688 preceding ripple contact (PRC) was the A36 contact and the SOC was concordant with the PRC.
 689 SI_m values scaled as black to red are statistically significant values to which the FWE-corrected
 690 threshold was applied. At ripple power increasing from the A36 contact, significant θ -ripple
 691 PAC were also observed (red arrow in D). First, significant θ -ripple PAC were observed (black
 692 bashed square in D), after that, significant δ -ripple PAC were observed (black bashed square
 693 in E). In this case, time lag between θ - and δ -ripple PAC were observed. During significantly
 694 high values of SI_m, the fluctuation of red circles changed at certain rhythms. We inferred that
 695 the rhythmic fluctuations were tuned at θ or δ rhythm, and represented the PAC phenomenon.
 696 The SO is 8:28:53. The 1 s, 26 s, and 46 s in Fig. 5F correspond to 8:28:54, 8:29:19, and 8:29:39
 697 in respectively. All implanted electrode contacts after removal of noisy contacts are shown in

698 the vertical axes (B, C, D, and E). The vertical bars indicating current-time are colored red in
699 iEEG signals (B), white in ripple normalized power (C), and blue in PAC (D, and E). The vide
700 was played at 1.5x.

701

702

Preprint

703 **References**

704

705 Akiyama T, Chan DW, Go CY, Ochi A, Elliott IM, Donner EJ, et al. Topographic movie of
706 intracranial ictal high-frequency oscillations with seizure semiology: epileptic network in
707 Jacksonian seizures. *Epilepsia* 2011;52(1):75-83.

708 Akiyama T, Otsubo H, Ochi A, Galicia EZ, Weiss SK, Donner EJ, et al. Topographic movie of
709 ictal high-frequency oscillations on the brain surface using subdural EEG in neocortical
710 epilepsy. *Epilepsia* 2006;47(11):1953-7.

711 Amiri M, Frauscher B, Gotman J. Phase-amplitude coupling is elevated in deep sleep and in
712 the onset zone of focal epileptic seizures. *Front Hum Neurosci* 2016;10:387.

713 Amiri M, Frauscher B, Gotman J. Interictal coupling of HFO s and slow oscillations predicts
714 the seizure - onset pattern in mesiotemporal lobe epilepsy. *Epilepsia* 2019;60(6):1160-70.

715 Ayoubian L, Lacombe H, Gotman J. Automatic seizure detection in SEEG using high frequency
716 activities in wavelet domain. *Med Eng Phys* 2013;35(3):319-28.

717 Canolty RT, Edwards E, Dalal SS, Soltani M, Nagarajan SS, Kirsch HE, et al. High gamma
718 power is phase-locked to theta oscillations in human neocortex. *Science* 2006;313(5793):1626-
719 8.

720 Cohen MX. Assessing transient cross-frequency coupling in EEG data. *J Neurosci Methods*
721 2008;168(2):494-9.

722 Cohen MX. *Analyzing neural time series data: theory and practice*: MIT press, 2014.

723 Dichter MA. Basic mechanisms of epilepsy: targets for therapeutic intervention. *Epilepsia*
724 1997;38:S2-S6.

725 Edakawa K, Yanagisawa T, Kishima H, Fukuma R, Oshino S, Khoo HM, et al. Detection of
726 Epileptic Seizures Using Phase-Amplitude Coupling in Intracranial Electroencephalography.
727 *Sci Rep* 2016;6.

728 Haegens S, Nacher V, Luna R, Romo R, Jensen OJPotNAoS. α -Oscillations in the monkey
729 sensorimotor network influence discrimination performance by rhythmical inhibition of
730 neuronal spiking. 2011;108(48):19377-82.

731 Hashimoto H, Hasegawa Y, Araki T, Sugata H, Yanagisawa T, Yorifuji S, et al. Non-invasive
732 detection of language-related prefrontal high gamma band activity with beamforming MEG.
733 *Sci Rep* 2017;7(1):14262.

734 Hashimoto H, Kameda S, Maezawa H, Oshino S, Tani N, Khoo HM, et al. A Swallowing
735 Decoder Based on Deep Transfer Learning: AlexNet Classification of the Intracranial
736 Electrocorticogram. *Int J Neural Syst*;0(0):2050056.

737 Hashimoto H, Khoo HM, Yanagisawa T, Tani N, Oshino S, Kishima H, et al. Coupling between
738 infraslow activities and high-frequency oscillations precedes seizure onset. *Epilepsia Open*
739 2020a;5(3):501-6.

740 Hashimoto H, Takahashi K, Kameda S, Yoshida F, Maezawa H, Oshino S, et al. Swallowing-

741 related neural oscillation: An intracranial EEG study. *bioRxiv* 2020b.

742 Ibrahim GM, Wong SM, Anderson RA, Singh-Cadieux G, Akiyama T, Ochi A, et al. Dynamic
743 modulation of epileptic high frequency oscillations by the phase of slower cortical rhythms.
744 *Exp Neurol* 2014;251:30-8.

745 Iimura Y, Jones K, Takada L, Shimizu I, Koyama M, Hattori K, et al. Strong coupling between
746 slow oscillations and wide fast ripples in children with epileptic spasms: Investigation of
747 modulation index and occurrence rate. *Epilepsia* 2018;59(3):544-54.

748 Ikeda A, Taki W, Kunieda T, Terada K, Mikuni N, Nagamine T, et al. Focal ictal direct current
749 shifts in human epilepsy as studied by subdural and scalp recording. *Brain* 1999;122(5):827-38.

750 Ikeda A, Terada K, Mikuni N, Burgess RC, Comair Y, Taki W, et al. Subdural recording of ictal
751 DC shifts in neocortical seizures in humans. *Epilepsia* 1996;37(7):662-74.

752 Imamura H, Matsumoto R, Inouchi M, Matsubishi M, Mikuni N, Takahashi R, et al. Ictal
753 wideband ECoG: direct comparison between ictal slow shifts and high frequency oscillations.
754 *Clin Neurophysiol* 2011;122(8):1500-4.

755 Jirsch J, Urrestarazu E, LeVan P, Olivier A, Dubeau F, Gotman J. High-frequency oscillations
756 during human focal seizures. *Brain* 2006;129(6):1593-608.

757 Kanazawa K, Matsumoto R, Imamura H, Matsubishi M, Kikuchi T, Kunieda T, et al.
758 Intracranially recorded ictal direct current shifts may precede high frequency oscillations in
759 human epilepsy. *Clin Neurophysiol* 2015;126(1):47-59.

760 Kitchigina VF, Butuzova MV. Theta activity of septal neurons during different epileptic phases:
761 the same frequency but different significance? *Exp Neurol* 2009;216(2):449-58.

762 Luo H, Poeppel DJN. Phase patterns of neuronal responses reliably discriminate speech in
763 human auditory cortex. *Neuron* 2007;54(6):1001-10.

764 Maris E, Oostenveld R. Nonparametric statistical testing of EEG- and MEG-data. *J Neurosci*
765 *Methods* 2007;164(1):177-90.

766 Modur PN, Zhang S, Vitaz TW. Ictal high - frequency oscillations in neocortical epilepsy:
767 implications for seizure localization and surgical resection. *Epilepsia* 2011;52(10):1792-801.

768 Nariai H, Matsuzaki N, Juhász C, Nagasawa T, Sood S, Chugani HT, et al. Ictal high -
769 frequency oscillations at 80–200 Hz coupled with delta phase in epileptic spasms. *Epilepsia*
770 2011;52(10):e130-e4.

771 Nonoda Y, Miyakoshi M, Ojeda A, Makeig S, Juhász C, Sood S, et al. Interictal high-frequency
772 oscillations generated by seizure onset and eloquent areas may be differentially coupled with
773 different slow waves. *Clin Neurophysiol* 2016;127(6):2489-99.

774 Ochi A, Otsubo H, Donner EJ, Elliott I, Iwata R, Funaki T, et al. Dynamic changes of ictal
775 high-frequency oscillations in neocortical epilepsy: using multiple band frequency analysis.
776 *Epilepsia* 2007;48(2):286-96.

777 Perucca P, Dubeau F, Gotman J. Intracranial electroencephalographic seizure-onset patterns:
778 effect of underlying pathology. *Brain* 2014;137(Pt 1):183-96.

779 Ray S, Crone NE, Niebur E, Franaszczuk PJ, Hsiao SS. Neural correlates of high-gamma
780 oscillations (60–200 Hz) in macaque local field potentials and their potential implications in
781 electrocorticography. *J Neurosci* 2008;28(45):11526-36.

782 Rodin E, Modur P. Ictal intracranial infraslow EEG activity. *Clin Neurophysiol*
783 2008;119(10):2188-200.

784 Schönberger J, Birk N, Lachner - Piza D, Dümpelmann M, Schulze - Bonhage A, Jacobs J.
785 High - frequency oscillations mirror severity of human temporal lobe seizures. *Annals of*
786 *Clinical and Translational Neurology* 2019;6(12):2479-88.

787 So N, Gotman J. Changes in seizure activity following anticonvulsant drug withdrawal.
788 *Neurology* 1990;40(3 Part 1):407-.

789 Wang S, Wang IZ, Bulacio JC, Mosher JC, Gonzalez - Martinez J, Alexopoulos AV, et al.
790 Ripple classification helps to localize the seizure - onset zone in neocortical epilepsy. *Epilepsia*
791 2013;54(2):370-6.

792 Weiss SA, Orosz I, Salamon N, Moy S, Wei L, Van't Klooster MA, et al. Ripples on spikes
793 show increased phase - amplitude coupling in mesial temporal lobe epilepsy seizure - onset
794 zones. *Epilepsia* 2016;57(11):1916-30.

795 Wu S, Kunhi Veedu HP, Lhatoo SD, Koubeissi MZ, Miller JP, Lüders HO. Role of ictal baseline
796 shifts and ictal high - frequency oscillations in stereo - electroencephalography analysis of
797 mesial temporal lobe seizures. *Epilepsia* 2014;55(5):690-8.

798 Yanagisawa T, Yamashita O, Hirata M, Kishima H, Saitoh Y, Goto T, et al. Regulation of Motor
799 Representation by Phase-Amplitude Coupling in the Sensorimotor Cortex. *J Neurosci*
800 2012;32(44):15467-75.

801 Zijlmans M, Jiruska P, Zelmann R, Leijten FS, Jefferys JG, Gotman J. High - frequency
802 oscillations as a new biomarker in epilepsy. *Ann Neurol* 2012;71(2):169-78.

803

Phase-amplitude coupling of ripple activities during seizure evolution with theta phase

Hiroaki Hashimoto. M.D., Ph.D.^{1,2,3*}, Hui Ming Khoo. M.D., Ph.D.⁴, Takufumi Yanagisawa. M.D., Ph.D.⁴, Naoki Tani. M.D., Ph.D.⁴, Satoru Oshino. M.D., Ph.D.⁴, Haruhiko Kishima. M.D., Ph.D.⁴, Masayuki Hirata. M.D., Ph.D.^{1,3,4}

- ¹ Department of Neurological Diagnosis and Restoration, Graduate School of Medicine, Osaka University, Suita 565-0871, Japan
- ² Department of Neurosurgery, Otemae Hospital, Osaka, 540-0008, Japan
- ³ Endowed Research Department of Clinical Neuroengineering, Global Center for Medical Engineering and Informatics, Osaka University, Suita 565-0871, Japan
- ⁴ Department of Neurosurgery, Graduate School of Medicine, Osaka University, Suita 565-0871, Japan

* Correspondence:

Hiroaki Hashimoto, M.D., Ph.D.

Invited Researcher, Department of Neurological Diagnosis and Restoration, Graduate School of Medicine, Osaka University, Yamadaoka 2-2, Suita, Osaka, Japan

Tel.: +81-6-6210-8429

Fax: +81-6-6210-8430

E-mail: h-hashimoto@ndr.med.osaka-u.ac.jp

Supplementary Figure 1

Supplementary Figure 1 Normalized power of the low frequency bands at the pre-ictal and ictal states.

The main low frequency band, coupled with ripple, was the δ band in 2/15 seizures (13%), θ band in 12/15 seizures (80%), and α band in 1/15 seizures (7%) (Table 1). For each seizure group with a different low frequency band (δ -ripple coupling in A, θ -ripple coupling in B, and α -ripple coupling in C), we compared the low frequency normalized power at the δ , θ , α , and β bands during the pre-ictal and ictal states using the Kruskal-Wallis test with Bonferroni correction. Except for the pre-ictal state of δ -ripple coupling, there were significant differences (corrected p values ($c.p$) < 0.05). In all three groups, during the pre-ictal state, the δ band tended to achieve the more values than others, however, during the ictal state, β band tended to achieve greater values than others. The main low frequency band that shows coupling with ripple doesn't match the low frequency band that shows power increasing.

